

Neutron Activation Analysis, A Titanium Material Study

Charles Dresser, Cara Henson, Jeremy Mock, Robert Svoboda, Matthew Szdagis and Mani Tripathi

Aug 17th 2010

Abstract

In order to obtain faster and more accurate measurements of radioactive contaminants within a sample of titanium we expose it to a neutron flux. This flux will activate the stable and quasi stable (those with extremely long half lives) isotopes into resultant daughter cells that are unstable which will result in shorter half lives on the order of minutes to days. We measured the resulting decays in the Germanium Crystal Detector and obtained a complex gamma spectrum. A mathematical model was used to recreate the production of the measured isotopes in the neutron flux and the resultant decays. Using this model we calculated the mass percent of the contaminate isotopes inside our titanium sample. Our mathematical model accounted for two types of neutron activation, fast or thermal activation, since this would determine which contaminate was the source of our signals. By looking at the percent abundances, neutron absorption cross-sections and the resulting mass percents of contaminate we are able to determine the exact source of our measured signals. Our results have verified that for fast neutron activation the method is very accurate; however, for thermal activation more calibrations to the testing procedure must be done before we can say it is a reliable measurement of mass percent contamination.

I. Introduction

Due to the nature of no background experiments it is necessary to know exactly what radioactive contaminant sources there are innately in the experimental set up. Typically, to determine upper limits on such background contaminants, samples are placed in heavily shielded Germanium Crystal Gamma Ray Detectors and left there for weeks to months until enough isotope decays have been detected. The long counting time is needed due to the fact that the quasi stable isotopes within the samples take millions to billions of years to decay away. This possesses a problem in time,

money due to cost of shielding and finally accuracy due to lack of signal¹.

The purpose of this research is to develop a method for determining radioactive contaminants within materials of interest (i.e. Titanium): contaminants such as Uranium, Thorium and Potassium. Additionally measure, within less time, absolute concentrations of the contaminants with Neutron Activation Analysis (NAA) and low background counting.

The reason Titanium was chosen was due to its use in the LUX dark matter detector. The detector will measure interactions between Xenon liquid and dark matter in a low background environment.

Though because the cryostat used to keep the xenon in liquid form is made of Titanium it is necessary to know what radioactive contaminants are present since they could give false readings in the LUX detector. Titanium does contain trace elements of Uranium, Thorium and potassium and in their present form they have extremely long half lives but are still sources of background radiation. Thus their concentrations must be known to a high precision.

II. Theory

Nuclei are composed of protons and neutrons. These particles have discrete energy levels that they exist in. Depending on the configuration of neutrons and protons these nuclei could be energetically unstable². In order to reach their ground state they can emit γ rays, β particles or α particles to release the necessary energy to become stable. Equation Set I expresses the possible decay modes.

Concerning α -decay the unstable parent nuclei emits a helium nucleus (the alpha particle) resulting in a daughter nucleus whose atomic number is two less than the parent and whose atomic mass is four atomic mass units less than the parents.

β -Decay has three different options, the emission of an electron, a positron or the capture of an electron. In the first case a neutron in the unstable parent nucleus decays into a proton, an electron and an antineutrino. The electron and the antineutrino are ejected out of the nucleus while the proton remains. Thus the daughter nucleus has an atomic number greater than the parent by one while the atomic mass remains constant.

In the second option, positron emission, a proton inside the nucleus of the parent absorbs the difference in binding energy between the parent and the daughter

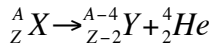
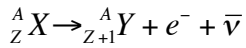
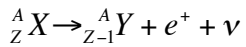
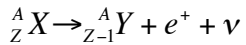
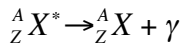
nucleus, which forces the proton to decay into a neutron, a positron and a neutrino. The positron and the neutrino are then ejected out of the nucleus and the neutron stays in the nucleus. The resultant daughter nucleus is one atomic number smaller but with the same mass as the parent.

The third option, electron capture, involves a proton in the parent nucleus absorbing an electron and the difference in binding energy between the parent and daughter nucleus. This causes the proton to decay into a neutron a positron and a neutrino. The resultant daughter nucleus is one atomic number smaller but with the same mass as the parent.

Finally the last form of decay we are considering is γ -decay. γ -decay occurs when a nucleus in an excited state of several MeV's. The emitted γ rays carry away the excess energy³.

There are several ways to excite nuclei to produce γ rays, one of which is beta decay. Figure I depicts an example of Cl-38 going through a gradual γ stepping to the ground state after a β -decay, also known as the decay scheme. The resultant daughter nucleus after beta decay typically has excess energy. The beta decay does not necessarily put the daughter nucleus into its desired ground state. Instead after the daughter nucleus is formed it then steps down through different γ decays to reach the desired ground state.

Each path will emit different γ rays carrying different amounts of energy with them. These γ 's are what the counting detectors will be reading. From the peak signals collected one could work backwards to determine what was the source of the γ ray. The probability of these decay paths occurring (Branching Ratios) determines how much of a particular signal one would collect in a detector sensitive to gamma rays.

Eqn_1: α - DecayEqn_2: β - Decay: (β^- , β^+ , e^- capture)Eqn_2a: β^- : (e^- emission)Eqn_2b: β^+ : (e^+ emission)Eqn_2c: e^- capture:Eqn_3: γ - Decay:

* = excited _ state

Equation Set I: Radiation Decay Modes³

Depicts through reaction equations the resulting products of α , β and γ decay.

The resultant spectrum from the gamma decays will directly reflect key characteristics of the source, as shown in Figure II below. It depicts the placement of counts (gamma decays that hit a gamma detector) versus energy of the incident gamma. Depending on the angle at which the decayed gamma hits the detector, the measured amount of energy will vary. This will cause counts associated with a particular isotope will be spread throughout a window of energy bins. See the detector set up later in this paper for the full apparatus description.

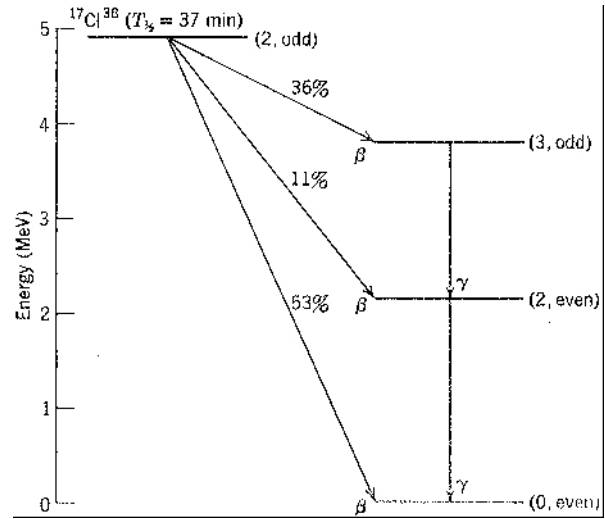


Figure I: CI-38 Decay Scheme

Here we can see the CI-38 decay scheme⁴. The vertical axis depicts the energy of the Parent as being the highest and with the resulting decays the energy decreases until the daughter nucleus ${}^{18}\text{A}^{38}$ is reached which has 0 MeV's making it the ground state. There are three possible paths the β -decay can take with respect to energy release.

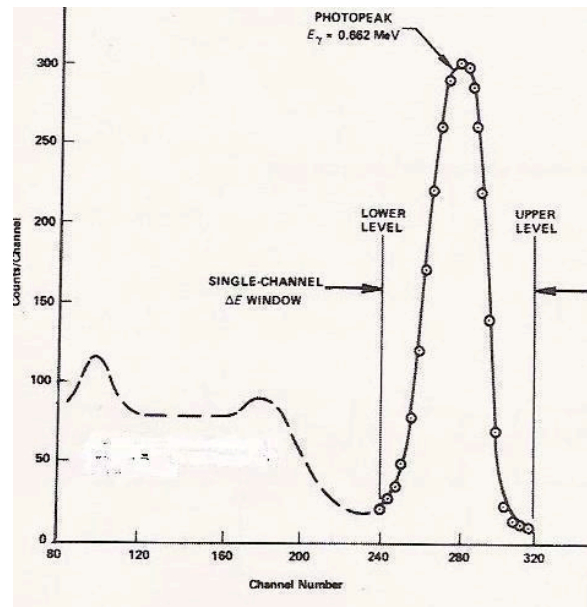


Figure II: ${}^{137}\text{Cs}$ Spectrum

⁶The distinct peak towards the far right is the photopeak, which is known as the full energy peak. It reflects the **incident photon energy (E_γ)** of the absorbed gamma rays. The plateau region reflects the Compton interactions that occur between the incident

photons and nearly free electrons, where the peak at the right edge of this region is the Compton edge.

The Compton edge shows the maximum energy that an electron can absorb through Compton interactions. This energy is a result of kinematic collisions between photons and nearly free electrons. Through laws of conservation of momentum and energy the photon loses some, or all of its energy and the electron in turn gains that energy. The Compton edge corresponds to the maximum resulting Kinetic energy absorbed by the electron, where

Eqn 4:

$$E_e = E_\gamma - E_{\gamma'}$$

And,

Eqn 5:

$$E_{\gamma'} = \frac{E_\gamma}{1 + 2E_\gamma(1 - \cos\theta)}$$

where,

$\theta = 180^\circ$ at the

photopeak energy.

$E_{\gamma'}$ is associated with the peak on the left of the plateau region, the backscattering peak, which is approximately equal to the **minimum energy scattered photon ($E_{\gamma'}$)** or the lower limit of the photopeak.

Thus knowing the theoretical energy of a source peak it is possible to determine how precise the actual measurements are for a particular detector by comparing.

In order to get a full efficiency spectrum you must use several different standard sources that have varying energy decay lines. For instance by looking at Cr-51, Ar-41, Mn-56 (which has two main peaks) spectrums all in the same geometry will make it possible to determine the efficiencies at energies, 320KeV, 846KeV, 1293KeV and 1810KeV. The more standard sources tested the clearer the efficiency curve will be.

Additional γ -decay counting

considerations include what is known as the dead time. Gamma ray spectrometers have a maximum response time. In other words it takes a certain amount of time for the signal to reach the multi channel analyzer. Between the time of incident energy and the reception of the signal in the computer the Germanium crystal effectively can't send off another signal. Thus if there is a very high rate of decays from the source, the detector only catches so many of the incident gammas.

In order to account for this dead time one must consider two different time stamps that the detector gives to the multi channel analyzer called live time and real time. Real time expresses how much time has passed between count start time and count end time. Live time reflects how long during the real time was the detector actually on. For example, if the real time was 2000sec and the live time was 1950sec we would have a 2.5% dead time that is approximately 50sec total that the detector was processing a signal and not reading new ones.

There are two ways that this needs to be taken into account, first in counting time considerations and then in theoretical recreations of decays. With concern to counting times, if the dead time is above 10% it is typically necessary to count for longer periods of time to allow the detector build up greater statistics; however, it is also possible to change the geometry set up so that the source is farther away from the detector. This increases the time for the gamma rays to traverse the distance from the source to the detector and in turn gives the detector more time to process its information and then receive a new signal.

In order to understand the second efficiency correction we must first consider how one builds theoretical model of a decay signal.

⁸Assuming you know exactly how much of a source you start with we can model the average number of decaying nuclei as the probability that any one nuclei will decay in a slice of time dt as shown in the following differential;

Eqn: 6

$$dN = -\lambda N dt$$

Where;

N is the number of undecayed nuclei at time t .

$$\lambda = \frac{\ln(2)}{t_{1/2}}$$

$$t_{1/2} = \text{half_life}$$

Separating variables and integrating this differential we will get the solution to our equation;

Eqn 7:

$$\int_{N(0)}^{N(t)} \frac{dN}{N} = -\lambda \int_0^t dt$$

gives;

$$N(t) = N(0)e^{-\lambda t}$$

Where;

$N(0)$ is the initial number of nuclei at $t=0$

$N(t)$ is the final number of undecayed nuclei at time t .

This solution depicts the number of surviving atoms after a time t ; however, in predicting what a detector will read, we want to see how many decays there actually were (signal counts). Thus by taking the difference of the initial mass of the source and the final mass the result is the number of decayed nuclei over a time t . This will make it possible to construct a curve depicting signal counts versus time. Where at any time the value of the signal is what one would

expect to see from a detector if it had 100% efficiency on all counts; however this is not the case. To truly match the empirical signal given by the detector the mathematically built signal will have to be multiplied by the detector efficiency at the respective energy peak and additionally the ratio of live time over real time to force your model to “miss counts” just as the detector will when measuring real data.

Thus between the detectors energy efficiency curve at a set geometry and the ratio of the live and real times it is possible to accurately recreate the detector signal assuming the initial mass and half-life of the source is known.

With all this in mind we can now consider methods for determining radioactive contaminants in samples of interest. We will be considering direct low background counting and the main method of interest involving neutron activation. We will first consider direct counting.

Low background direct counting requires two main parameters, time and shielding. Non-radioactive samples (such as plain titanium) have within them fairly stable radioactive contaminants. These isotopes have half-lives on the order of millions to billions of years. This means that the probability of detecting decay is very small. Thus in order to obtain a small blip of a signal it is necessary to let a detector count the sample for weeks to months. At the end of the counting, depending on the concentration of the contaminants, there might be a peak seen or there will just be a flat line. If there is a peak then that is a direct measurement and it can reveal exactly how many parts per million (ppm) there are present within the main sample⁹. If no peak is seen, which is typically the case, then it is possible to place an upper limit on the contaminant. A good estimation of the expected signal counts is to take the square

root of the background continuum. This is effectively a one sigma error in the measurement of the background. A fluctuation that could either be caused by the background radiation or by the expected signal. Using that number, as the maximum number of signal counts possible then it is a matter of working backwards to determine the mass of the radioactive contaminates. We will discuss this upper limit process in greater detail in the NAA data analysis section.

The main problems with direct counting are time and accuracy. Counting times are absurdly long and most of the time, when dealing with small concentrations, the best measurement possible is an upper limit. Upper limits in experiments that call for a precise measurement of the systems background are not enough. This leads us to our method of choice for development, Neutron Activation Analysis.

The Neutron Activation Analysis Theory and Method

Instead of direct counting and waiting for one or two random decays to occur, this method forces the stable nuclei to become unstable and decay much faster. This is done through neutron activation. Figure III shows the experimental set up for neutron activation.

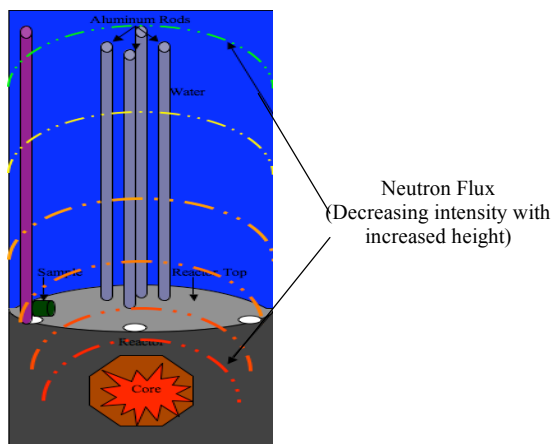


Figure III: Experimental Set Up

The sample is exposed to a neutron flux that radiates out from the reactor core in decreasing intensity with increased height from the core. The neutrons bombard the sample (which is placed some set distance above the top of the reactor) and the resulting collisions activate the isotopes in the sample and cause them to become unstable.

¹⁰There are two types of neutron activation, Fast and Thermal. The two cases depend on the kinetic energy that the neutrons collide into a nucleus with.

Concerning Thermal Neutron Activation the bombarding neutrons approach the nucleus with a kinetic energy of $1/40\text{eV}$'s. The neutron "slowly" floats in and is absorbed by a parent nucleus. The mass number of the nucleus increases by one and the atomic number remains constant. The increase in mass and kinetic energy produces an excited daughter nucleus. The daughter γ -decays to reach a ground energy state; however, because this daughter nucleus is still unstable it will decay further to reach an even lower energy state. In the case of our Titanium material study the result decay will be a β^- or double β^- -decay. The resultant β decay will lower the nucleus atomic number by one but maintain the new atomic mass. This second daughter nucleus will also be in an excited state and will γ -decay in order to reach a new ground state for the element it has decayed into. This can continue on for several decays until a final daughter nucleus is energetically stable.

With concern to Fast Neutron Activation the bombarding neutrons collide with the parent nucleus with a kinetic energy of 1MeV . The collision transfers enough energy to the nucleus to knock off a proton, emit a gamma to compensate for the excitation and simultaneously absorb the neutron. The resultant daughter nucleus has the same mass as the parent but its atomic number has decreased by one. The resultant

daughter nucleus after emitting the gamma is in the ground state for the element it has become; however, its nucleus is still not energetically at the ground state. It will in turn β decay until it has reached a daughter nucleus that is stable, all the while emitting gammas along the way. Figure IV depicts these interactions with respect to Uranium-238 and Titanium-48 pictorially and through nuclear equations.

Thermal Neutron Activation: U-238

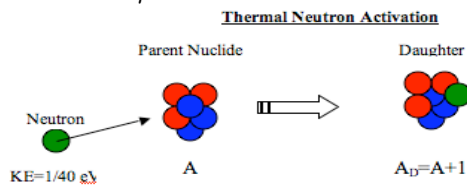
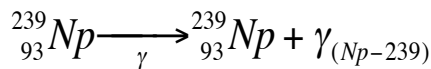
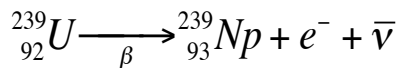
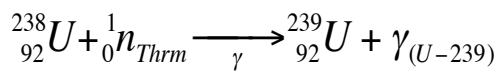


Figure IV a): Thermal and Fast Neutron Activation:

Here you can see from the equations the first activation, the γ -decay, the β -decay and finally the γ -decay of the daughter nuclide. The cartoon depicts the first step in the activation process before the first γ is emitted. This does not reflect the end of the decay chain. Np-239 will in turn decay further.

Fast Neutron Activation: Ti-48

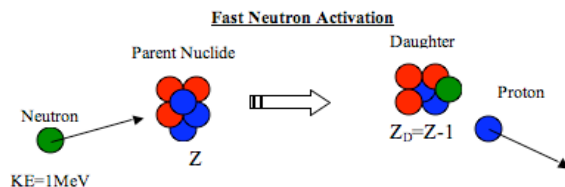
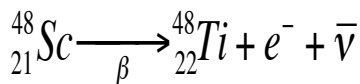


Figure IV b): Thermal and Fast Neutron Activation:

Here the equations depict the first activation, γ and finally the β -decay. The formed Ti-48 is a fairly

stable nuclide and thus is less likely to go through beta decay within a short time period. This decay chain basically holds here for some time. The picture shows how the fast neutron knocks off the proton.

The samples are left exposed to this neutron flux for a set time, lets assume 1hr after which there will be a cool off period between the end of the exposure and the beginning of decay counting in the Germanium detector.

One problem with this method is, upon getting the gamma spectrum, how to determine whether a daughter nucleus comes from fast or thermal activation. This is very important for determining the percent composition of radioactive isotopes since they are the sources for the daughter nuclei measured in the gamma spectrum data. For example Mn-56 can come from thermal activation of Mn-55 or from fast activation of Fe-56. There are three main properties about the parent nuclei that are used to determine this.

First we would consider the percent abundance of the proposed parent nucleus. Continuing with Mn-56 as our nucleus of interest, we might see that percent abundance of Mn-55 was 0% and Fe-56 was 100% abundant. This would immediately reveal that Mn-55 would not be the source of the Mn-56 daughter cell; however, this is not the true case. In reality Mn-55 has 100% and Fe-56 has 91% abundance. Thus if both parent candidates are equally likely we would then look at the probability that the parent nuclei would absorb either the fast or thermal neutrons. This probability is known as the nucleus neutron cross section expressed in units of barns.

Fe-56 for fast neutrons has a cross-section less than 1 barn depending on the energy (for fast neutrons the cross-section is energy dependent.) Mn-55 for thermal neutrons has a cross-section of 13.3 barns. Mn-55 seems like a very good candidate;

however, there is still one more check to consider.

If available, consult the chemical composition of your sample. For example in this instance it is known that .03% of the sample is made up of Iron. Thus we must first predict the production of the Mn-56 from Fe-56 and the subsequent decay scheme. Then match our predicted signal counts to match an observed signal from the detector with a mathematical representation of what's happening. If approximately .03% of Fe produces theoretically the same number of counts observed then you can be sure that the majority of the Mn-56 is coming from Fe-56 and not Mn-55. If not, then Mn-55 is your source and you determine the concentration result by working backwards to determine how much Mn-55 would be needed to create the measured signal.

With these methods in mind it is then important to understand how to model mathematically the production and decay schemes of isotopes throughout the NAA method. With this model we will then be able to determine the percent composition of any radioactive isotope that we can measure, or set an upper limit on those we do not see but expect to.

The Mathematical Model:

Let us consider the production of K-42 from thermal activation of K-41.

While in the reactor:

Eqn 8:

$$N_{K42}(T) = \int_{t=0}^{t=T_{\text{exp}}} (\Phi \sigma_{K41} N_{K41} - \lambda N_{K42}) dt$$

Where $N_{K42}(T)$ is the net number of K-42 produced over the exposure time (T_{exp}) after taking into account the amount that decayed in the same time period.

Φ = the neutron flux with units Neutrons/cm²/sec

σ = the absorption cross-section with units 1/cm²

$$\lambda = \frac{\ln(2)}{t_{1/2}} \text{ with units 1/sec}$$

N_{K42} = the number of K-42 produced in a time slice dt in units of atoms

N_{K41} = the number of K-41 initially present in units of atoms

While out of the reactor:

Eqn 9:

$$N_{K42}(t) = \left(- \int_0^t \lambda N_{K42}(T) dt \right)$$

Which shows the surviving number of K-42 after exposure. Now what the detector would see if there was no cool off time is as follows.

Eqn 10:

$$\Delta N_{K42}(t) = \left(N_{K42}(T) - \int_0^t \lambda N_{K42}(T) dt \right)$$

Where ΔN_{K42} is the number of decays from the end of the exposure to some time t . This reflects what your detector would see if there was no cool off period between the end of the exposure and the actual start of the counting. Thus what the detector sees is more explicitly,

Eqn 11:

$$\Delta N_{K42}(t) = \left(\int_0^{t_{\text{cool}}} \lambda N_{K42}(T) dt - \int_{t_{\text{cool}}}^{t_{\text{count}}} \lambda N_{K42}(T) dt \right) * B.R. * \%e_e$$

Where B.R. is the branching ratio, which is the probability that K-42 will γ -decay through a particular energy step.

$\% \text{eff}_{\text{detector}}$ = the detector efficiency which takes into account geometry, energy efficiency and the f_{live} (the ratio of live time over real time).

This gives you a recreation of the collected signal that the detector will show at the end of counting starting from the end of the cool off time. A graphical representation of the production and

resultant decays of K-42 and Mn-56 is depicted below in figure V.

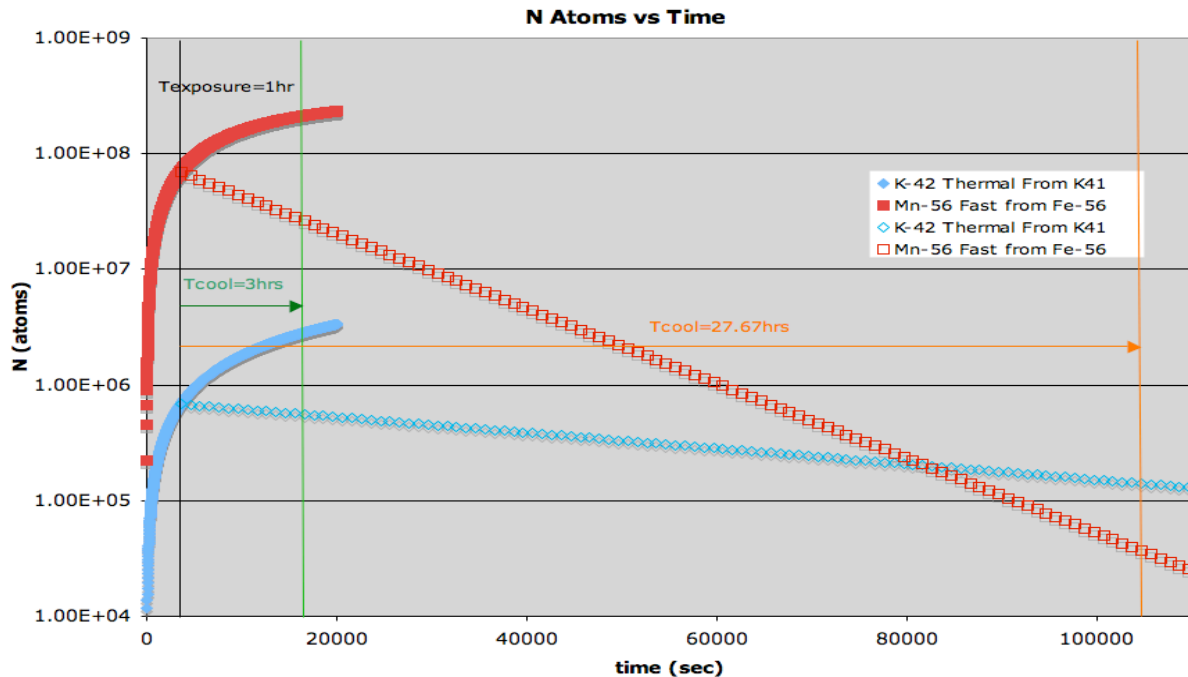


Figure V: Production and Decay of Mn-56 and K-42

This graph depicts the number of K-42 (blue lines) and Mn-56 (red line) that are present at all stages of the experiment. The thick blue and red curves depict the production of K-42 and Mn-56 inside the reactor. The vertical black line represent then end of the neutron flux exposure. The blue and red lines starting from the end of the exposure (the black line) show the surviving number of K-42 and Mn-56 as they decay over time. The green and orange vertical lines reflect when the sample would be placed for counting.

The two different cool off times show that if you wait only three hours there are still a large number of Mn-56 present. Starting the count after 3hrs will give you plenty of signal to measure Mn-56; however, if both Mn-56 and K-42 are in the same sample and your goal is to measure K-42 it may be prudent to wait 27hrs so that there is more K-42 than Mn-56. This is beneficial since Mn-56 will produce a Compton scattering continuum that will hide small amounts of potassium. By waiting 27hrs the Mn-56 will have mostly decayed away. This shows how sometimes it is

beneficial to wait to count your sample depending on what you are looking for.

The Neutron Flux

In order to decided the proper placement of a sample near a reactor it is necessary to know the intensity of thermal and fast fluxes at varying heights from the top of the reactor.

To determine the neutron flux, for both fast and thermal neutrons, two different flux markers (Ni, and $\text{Na}_2\text{CO}_3 \cdot \text{H}_2\text{O}$) were placed by the McClellan Nuclear Reactor Center (MNRC) team at three different

heights from the top of the reactor (0cm, 15cm, 30cm). Appendix A shows the flux report that was calculated and produced by Hungyuan B Liu of the MNRC group. His results from two different runs are listed

Run	Height (cm)	ϕ Thermal Neutrons/cm ² /sec	ϕ Fast Neutrons/cm ² /sec	ϕ Thermal/ ϕ Fast
1	0	7.9×10^{10}	6.9×10^9	11.4
1	15	4.5×10^9	1.0×10^9	4.50
1	30	5.1×10^8	2.1×10^8	2.43
2	0	6.3×10^{10}	6.0×10^9	10.5

Table I: Reactor Flux Measurements

As height from the top of the reactor is increased, both thermal and fast flux is dramatically reduced due to the water between the reactor and the samples. The highest thermal and fast flux readings are at the top of the reactor. The MNRC report however, did not include error bars on the flux measurements. Thus at some point we will have to either recalculate these values with estimated error or redo the flux measurements.

Because we are dealing with Titanium and looking for Uranium, Thorium and Potassium contamination we need to choose a height with a high enough intensity of thermal flux while at the same time have as little intensity of the fast flux as possible. The reason being that Titanium, when fast-activated, produces Scandium which will potentially hide other signals we wish to see. For instance Uranium and Thorium decay lines produced from thermal activation could be hidden by the backscatter continuum produced by the various Scandium lines if enough Titanium is fast activated.

Our height of choice was chosen to be 0cm above the top of the reactor given that it had the highest ratio of thermal to fast flux. Putting our samples directly into the reactor was not an option due to the fact that the fast flux would be extremely high in comparison to directly outside the reactor.

The Detector Set up:

In order to identify and analyze a particular source of radiation, one must be able to measure the energy that is incident upon a detector. Where, a Geiger Mueller

below Table I and are used as our basis for the neutron flux of the reactor for any further exposures that were run at 1.5MW capacity.

Counter only provides the count rates of incident radiation, a gamma spectrometer will provide energy measurements as well. In measuring the incident energy it is possible to build a gamma spectrum that will reveal the characteristics of radioactive nuclei that decayed to produce gamma rays. Figure VI shows a block diagram of a typical detector.

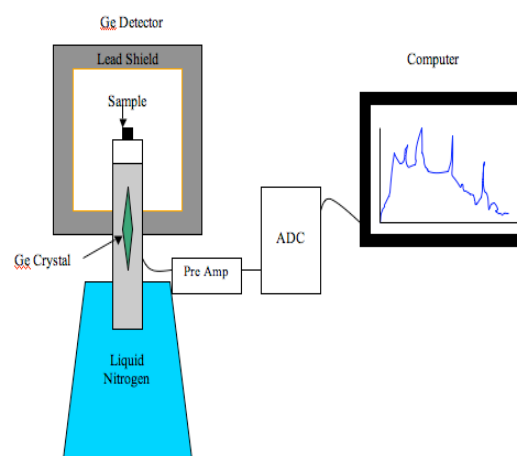


Figure VI: A Semiconductor Detector

Here we see a block diagram of the detector set up. The sample is inside a lead shield and placed near a germanium crystal. The crystal absorbs incoming gamma rays creating a current that flows to a pre amp, an ADC and finally a multi-channel analyzer.

The gamma spectrometer used is a solid-state detector. The detector itself maintains an electric field that surrounds a cathode and anode attached to the ends of a germanium crystal. A signal current is created by an incident gamma ray hitting a fixed electron in the valence band and exciting it into the conduction band. Now free to move around the electron can follow the influence of the electric field and flow to the positive anode. The hole left by the excited electron (effectively a positive charge) will in turn flow towards the negative cathode by means of one electron after another jumping to fill in the hole left behind by the other. With the freed electron and hole hitting their respective contacts a signal current is made. Any Signal Current created between the anode and cathode will flow to a pre amplifier, an Analogue to Digital Converter (ADC) and finally into the Multi Channel Analyzer software in the computer to produce a spectrum⁵.

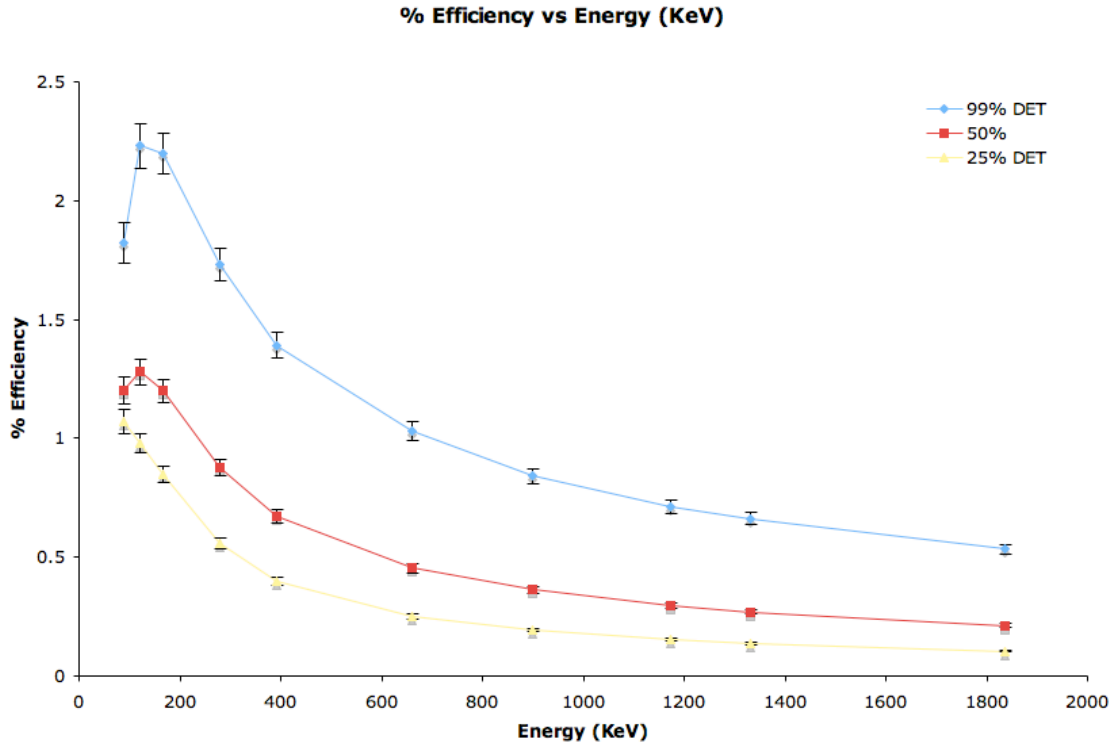
With respect to the figure above we see that the sample is placed in a six-inch lead shielding. The shielding prevents local and cosmic background radiation from producing false signals in the germanium detector. Additionally the samples placement inside the shield is important. The source of gammas needs to be in a position such that its geometry can be taken into account. A detectors' efficiency is dependent upon several aspects including the geometry of the sample placement.

In order to determine any detectors efficiency one must always refer to a known

source standard. For instance, if you have a radioactive point like source that needs to be 10cm away from the top of the Germanium crystal detector, then in order to determine the efficiency of that placement one must first count a known source in that same placement. By comparing what you expect to see energy wise in the signal peak versus what you actually measure, you can pull out the detectors efficiency with that geometry. An efficiency curve must be built up from similar comparisons at different energy levels.

Energy Calibration:

The software used to analyze the germanium crystal detector signals in our experiment is a Canberra product called Apex. The MNRC team conducts regular energy and geometry calibrations for this detector. In conducting their calibrations they have a single source with various known isotopes in it. The program reads in the signal from the detector, which originally reflects decay counts versus channel. The program empirically checks the location of the known peaks and converts the channel numbers into an energy. The MNRC possesses four different germanium detectors and they are labeled as the 99%, 50%, 25% and 8% detectors. The percent refers to the efficiency of the detectors when compared to a 3inch by 3inch NaI crystal detector. The provided energy calibrations for the three detectors used (99%, 50%, and 25%) are as follows in Graph I.

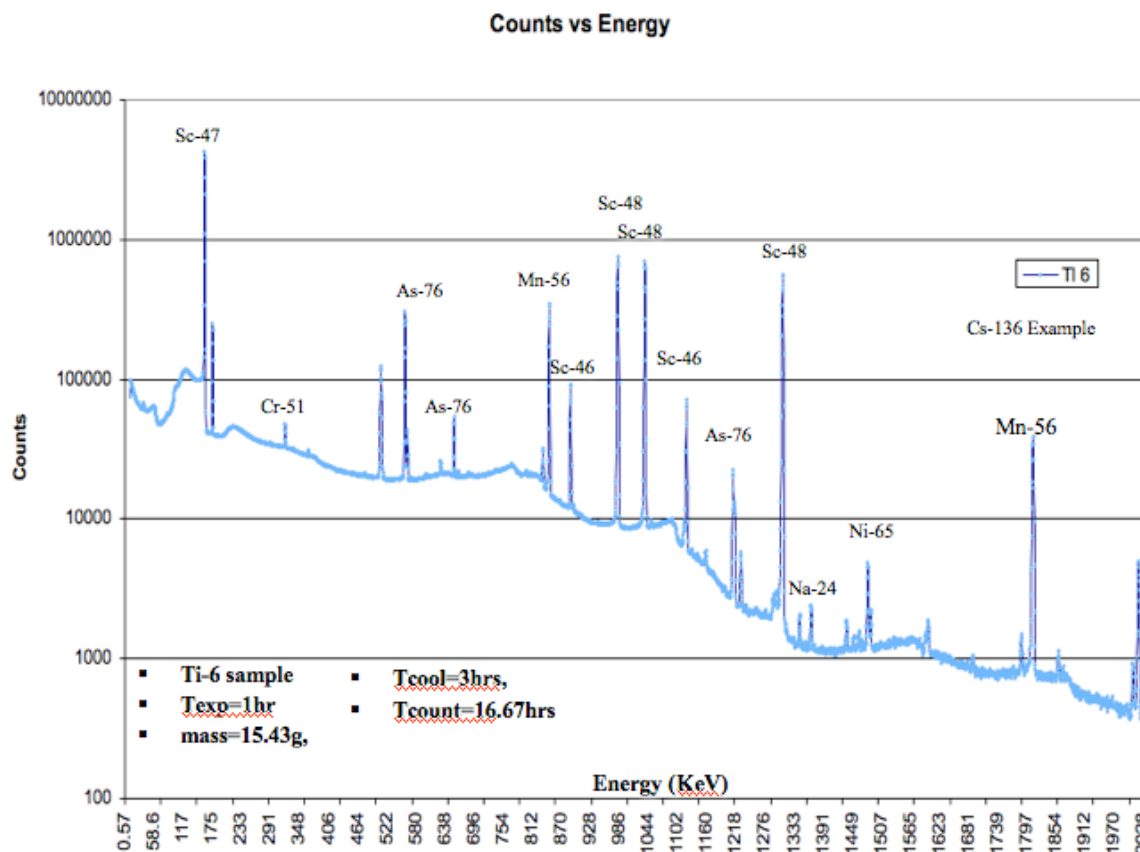


Graph I: Detector Efficiency Curves

This graph shows the % efficiency of the three detectors at various energies, where the 99% DET is the blue curve, the 50% DET is the red curve and the 25% DET is the yellow curve. The lines connecting the points are to guide the eye and do not reflect actual data points. The error bars are also given by the Apex program.

Data Analysis:**Raw Data**

A typical Exposure is expressed below in Graph I.



Graph II: Titanium Sample Gamma Spectrum Graph I depicts a typical Ti gamma spectrum after a 1hr exposure time, a cool off period of 3hrs and a total count time of 16.67hrs. The vertical axis represents the number of decays detected by the germanium counter over 16.67hrs. The horizontal axis is the respective energies that each gamma hit the crystal with.

The various Sc peaks provide considerable backscatter continuums that make the energy peaks of contaminants such as Thorium and Uranium not visible. Additionally we are also looking for the level of K contamination. What we expect to see is the K-42 1524KeV decay line from thermally activated K-41; however, that peak is hidden by the Mn-56 backscatter continuum. The peak at 511KeV results from cosmic rays hitting the germanium crystal and is not reflective of any contaminants inside the titanium. The Na-24 line was eventually discovered to be from human sweat deposited onto the Ti sample

during handling. This peak has been as minimized as much as possible by intense sonic bath cleaning with Isopropyl, Acetone and Distilled water.

Verification of NAA Method:
Iron concentration in Ti sample:

According to the Ti manufactures, the Ti samples we have been exposing possess .03% Fe which translates into 300ppm of Fe in Ti. We know that Fe-56 can fast activate into Mn-56; however so can Mn-55 through thermal activation. Thus our first step would be to confirm that our method could confirm

the concentration of Fe in the sample Ti. Table II expresses the results of our calculations, using the two decay lines (1810KeV and 847.6KeV) of Mn-56 seen in the gamma spectrum as crosschecks.

<u>Mn Decay lines</u>	<u>Fe Theory ppm</u>	<u>N Theory</u>	<u>N Observed</u>	<u>Fe ppm Observed</u>	<u>Avg Fe ppm Observed</u>	<u>Error of Avg ppm</u>
1810KeV	300	49,000	39,000	234	272.58	9%
846.75KeV	300	290,000	337,331	311		

Table II: Fe Concentration

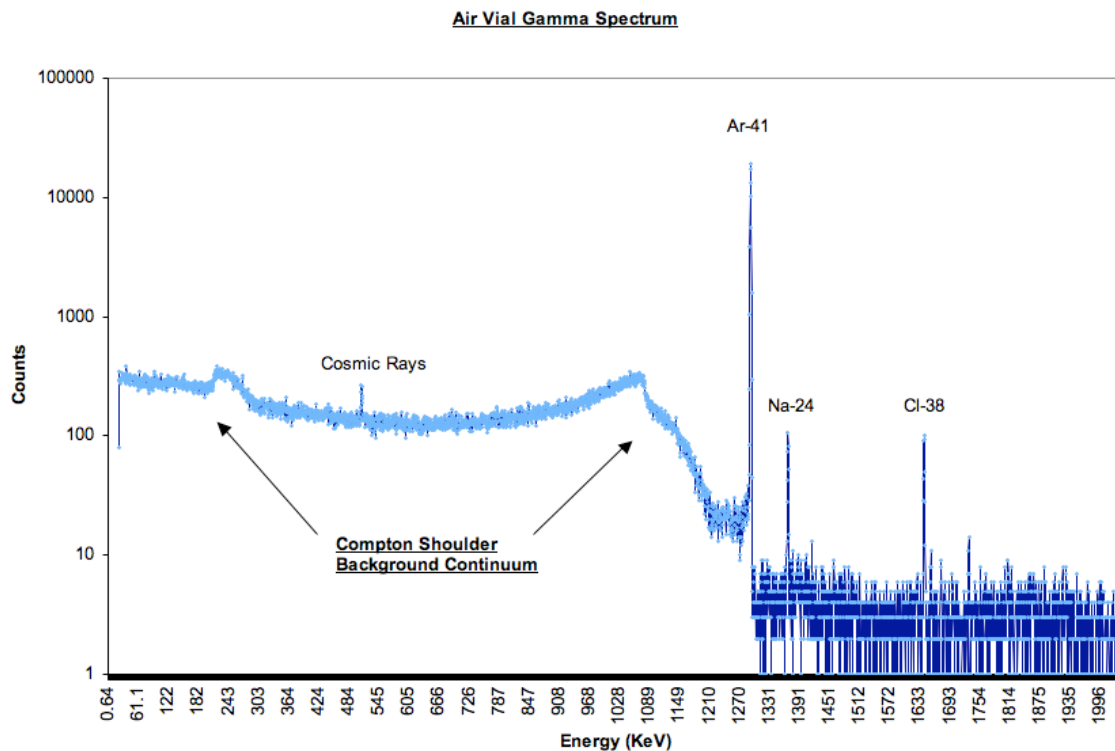
Table II depicts the theoretical ppm of Fe, measured by chemical analysis, along with our calculated ppm of Fe from observed counts.

Using the mathematical model and fast flux measurement described earlier in the report, we calculated how many counts we would have expected to see if 300ppm of Fe was fast activated into Mn-56 and then compared it with what was actually observed. The N observed was pulled directly from the raw data and is representative of the peak area. Between the two peaks we found that the average Fe ppm was 272.58ppm, which is 9% off from the theorized value.

This confirms that the source of the Mn-56 peak is indeed the .03% of Fe present in the Ti sample and confirms the Fast Flux measurement made by the MNRC team.

Argon Concentration in an Air Vial:

In order to test the reliability of the measured thermal flux we also exposed a vial filled with only air. Sticking this in the same position as the Ti samples we will activate the Argon in the air and knowing the dimensions of the vial we can calculate the amount of Ar in the vial and how much our mathematical model predicts when looking at the number of counts observed. The Air Vial spectrum is shown below in graph III and the subsequent ppm of Ar results are summarized in Table III.



Graph III: Air Vial Spectrum

Here we can see a clear Ar-41 peak at 1293 KeV and its resulting background continuum. Additionally there is a Na-24 and Cl-38 peak. These are a result of human sweat and the plastic that the vial is made up of. Because Ar-41 is so large in comparison to the Na and Cl peaks they do not inhibit our measurements of Ar and thus were not necessary to get rid of them through proper cleaning and the use of a different vial which might not have produced the Cl line.

The observed area of the Ar-41 peak was 72,500 counts. First we calculated the mass of air inside the vial. The dimensions of the vial are 2 inches in height with a radius of .3 inches. This gives a volume of 9.27cm^3 . Knowing the density of air is $.001275\text{g/cm}^3$ we determined there was $.011815\text{g}$ of Air in the vial. Knowing that the mass percent of Ar in air is $.674\%$ we found there was $.0000796\text{g}$ of Ar in the vial. This tells us that there is 6740 ppm of Ar in the air vial. Using our mathematical model we worked backwards to find the necessary Ar ppm in the vial to produce 72,500 counts is 2200ppm. 2200ppm of Ar in $.011815\text{g}$ of Air shows we would need $.0000796\text{g}$ of Ar. This 66.9% off from the theoretical calculation of the 6740 ppm of Ar in the vial

of Ar. This data Summary is shown below in Table III.

One possible reason for error is that the flux is over estimated for thermal interactions. According to our counterpart from Berkeley (Alan R Smith) it is possible that flux markers could possess resonances that would over estimate the flux measurement. We can confirm this with the Potassium concentration measurements, which will be discussed in the next section. It is interesting to note that we did not see this problem of resonance with the fast activation of Fe-56. The Fe measurement was only 9% off, less than a factor of 2 off. These resonances might not occur with the fast activation or we were lucky in not hitting that resonance. More evaluation must be done to confirm this.

It is also possible that vial was not fully sealed and some air may have leaked out cause the underestimation of the Ar ppm.

<u>Ar ppm Theory</u>	<u>Peak Area Observed</u>	<u>Ar ppm Calculated</u>	<u>Error</u>
6740	72,500	2200	66.9%

Table III: Ar ppm determination

Overall the estimated Ar ppm is off by a factor 3. This exposure must be repeated with a more securely sealed Air vial to ensure no air escape. More talk about what else needs to be done is reflected in the Future Work section at the end of this paper.

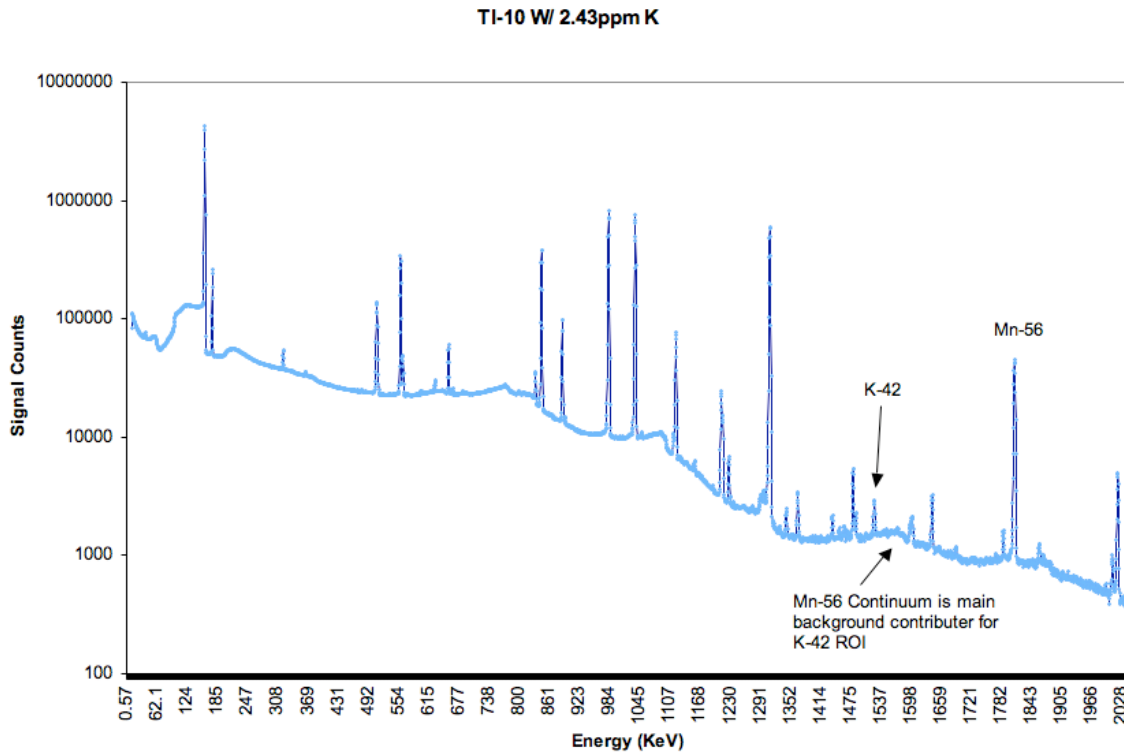
Potassium Concentration in Ti Sample (Part I, Addition of known amount)

Here we attempted to add known amounts of potassium to confirm our level of precision. Two solutions of KOH were made. The first solution had .034g KOH added to 150ml of de-ionized water and the second solution had .0037g KOH added to 150ml of de-ionized water.

First .25ml of the first solution was placed on top of a Ti sample labeled Ti-10 whose mass is 16.22g. Then .25ml of the second solution was added on top of a Ti

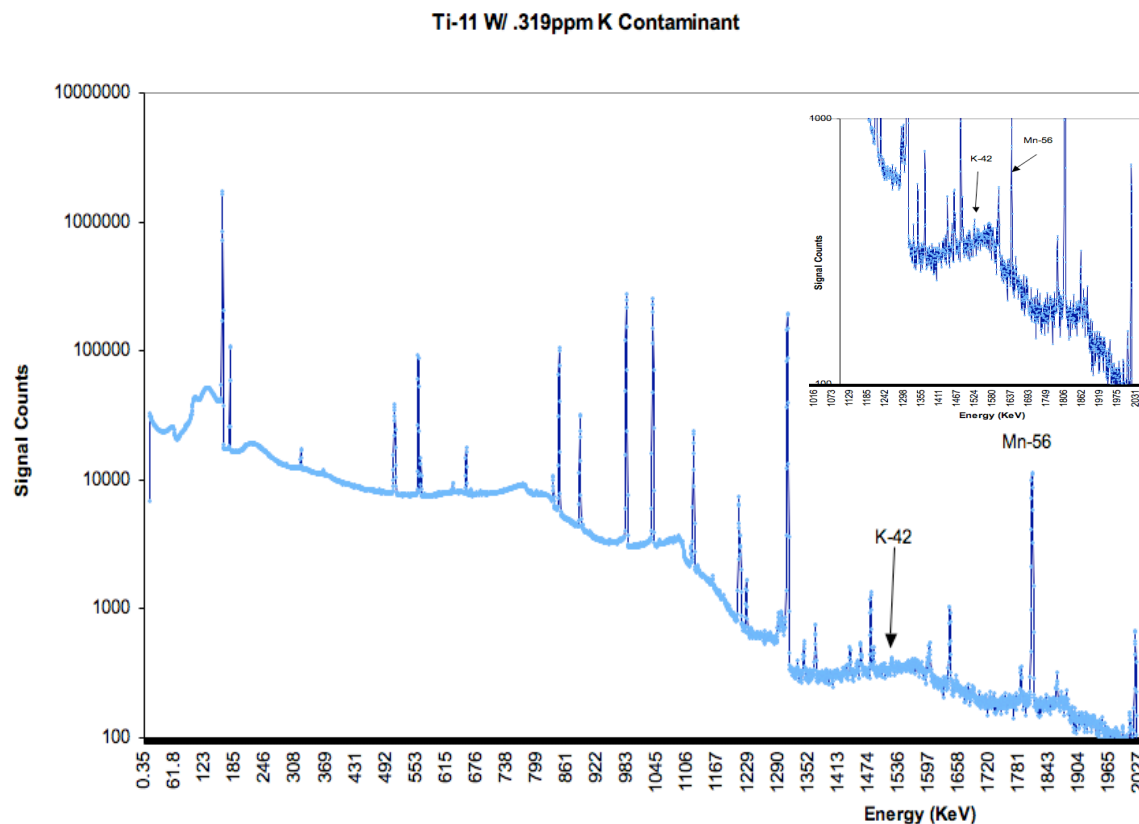
sample labeled Ti-11 whose mass is 12.93g. This results in us adding 2.43ppm of K on Ti-10 and .319ppm of K onto Ti-11.

These samples were exposed for an hour and then counted after a cool off period of 3hrs and then again at 23 hrs and 28min. The resultant Spectrum for Ti-10 is shown below in Graph IV, the spectrum for Ti-11 is exactly the same except the K peak is about a factor 10 smaller, shown in graph V. The resultant calculations of Kppm from observed data is displayed below in Table IV:



Graph IV: Ti-10 with 2.43ppm K Contaminant

Here we can see the gamma spectrum from the Ti-10 sample with a cool off time of 3hrs. The peaks seen match those as shown before in the beginning of the data analysis; however, this time the K-42 peak is indeed visible. This shows that it is possible to measure about a 2ppm contamination of K. See table IV and its description for exact results.



Graph V: Ti-11 W/ .319ppm K Contamination

Here we see the gamma spectrum of the Ti-11 sample with a cool off time of 3hrs. The K-42 line is barely visible. To show more explicitly that the line is indeed there the inset in the top right corner shows a zoomed-in section of the peak. It is evident that it is possible to see a peak from K contamination around .3ppm; however as shown from the data below the error is very high for reasons, which will be discussed shortly.

<u>Ti sample (cool time)</u>	<u>K ppm Theory</u>	<u>Peak Area Observed</u>	<u>K ppm Calculated</u>	<u>Error</u>
Ti-10 (3hrs)	2.43	8960	2.62	7.3%
Ti-10 (20hrs and 10 min)	2.43	3030	2.35	3.4%
Ti-11 (3hrs hrs)	.319	310	.125	60%
Ti-11 (20hrs and 10 min)	.319	188	.187	42%

Table IV: K ppm Determination

Table IV depicts ppm of K added to Ti sample and compares it to our calculated ppm of K from observed counts. Two separate measurements with two different cool off times were made to check for consistency.

Here we see that for the Ti-10 sample the measured error in ppm of K gets worse with decreasing concentration. This could be a reflection of either the limitation of the method (we might be able to only get within a factor 2 or 3 of the actual value at

really low concentrations) or an error in the addition of the known source solutions. Since KOH reacts with the water in air, its mass will continually change as water is absorbed. This changing mass was not accurately taken into account when the

solution was made. This could account for the large percent error in the Ti-11 Kppm. Since there was such a small amount of K (.0037g) being weighed for the second solution it may have been completely saturated much faster than the larger mass of KOH (.034g) before they were mixed into solution. It is possible that the larger .034g mass of KOH did not completely saturate before being mixed into solution and thus the mass weighed more accurately reflected the actual amount of KOH put into solutions (thus the smaller percent error).

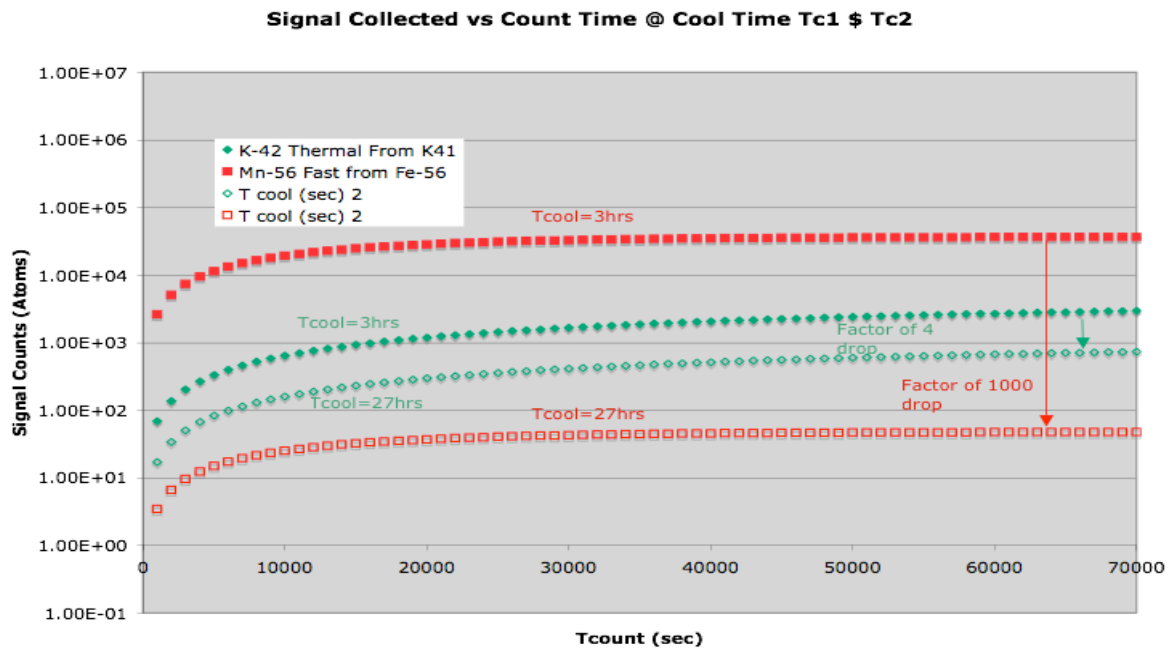
Measuring the Ti-10 and Ti-11 samples after a cool of about 24hrs we were still able to observe the K-42 line above the residual Mn-56 backscatter continuum. Graph VI shows how the signal intensity of

Mn and a 1ppm K contamination decrease with time. With less of the Mn-56 continuum present after one day the measured K-42 peak is more accurate in both cases; however, the smaller contaminate (the .319ppm) is still off by a considerable amount.

Despite these errors, this does show us that we can measure within the right magnitude of ten and at least within a factor of 3 of the actual ppm of the K isotope. This is in agreement with our Ar-41 measurement in that we are accurate to at least a factor of three. Though before these results can be considered valid this experiment must be repeated with a more accurate measurement. This will be further discussed in the section titled Future Work.

Graph VI: Signal Counts vs Count Time

Here with 1ppm K and 231ppm of Mn (Texposure=1hr) 15g sample



Graph VI: Signal Counts vs Count Time This depicts the signal intensity of K-42 (1ppm) and Mn-56 (231ppm) Here we can see why the added K is still visible even after 24 to 27 hrs. The intensity of the K-42 signal does drop by a factor of 4 but the Mn-56 line drops by a factor of 1000 over 27hrs. Thus measuring after 24 hrs would still allow you to see the K-42 peak with less Mn-56 continuum obscuring the K-42 peak.

Potassium Concentration (Part II, Verification of Direct Measurement)

According to Alan Smith at UC Berkeley (who conducted a direct low background count of our titanium samples before hand) the Ti sample we have been dealing with has a natural K contamination of .24ppm.

Upon exposure on a cleaned Ti sample (Ti-6) it was found that the K-42 line could not be seen at all, neither after 3hrs nor after 27hrs. the K-42 line signal intensity seemed to always be below the continuum background. Thus we decided to set and

upper limit and compare to the direct measurement done in Berkeley. By taking the region of interest (ROI) for the K-42 line and using one standard deviation of the background in that region we estimated the maximum amount of signal possible. The square root (1 sigma) of the background effectively shows that in the ROI the number of counts fluctuates by 1 sigma. This fluctuation is either caused from background fluctuations or the max possible signal from the K-42 line. Table V summarizes the results found.

<u>K-42 Expected Decay line</u>	<u>K ppm Theory</u>	<u>N Theory</u>	<u>N Observed</u>	<u>Kppm Calculated</u>	<u>Error K ppm</u>
1524.70KeV	.24ppm	666	50	.0180	92%

Table V: K ppm Determination

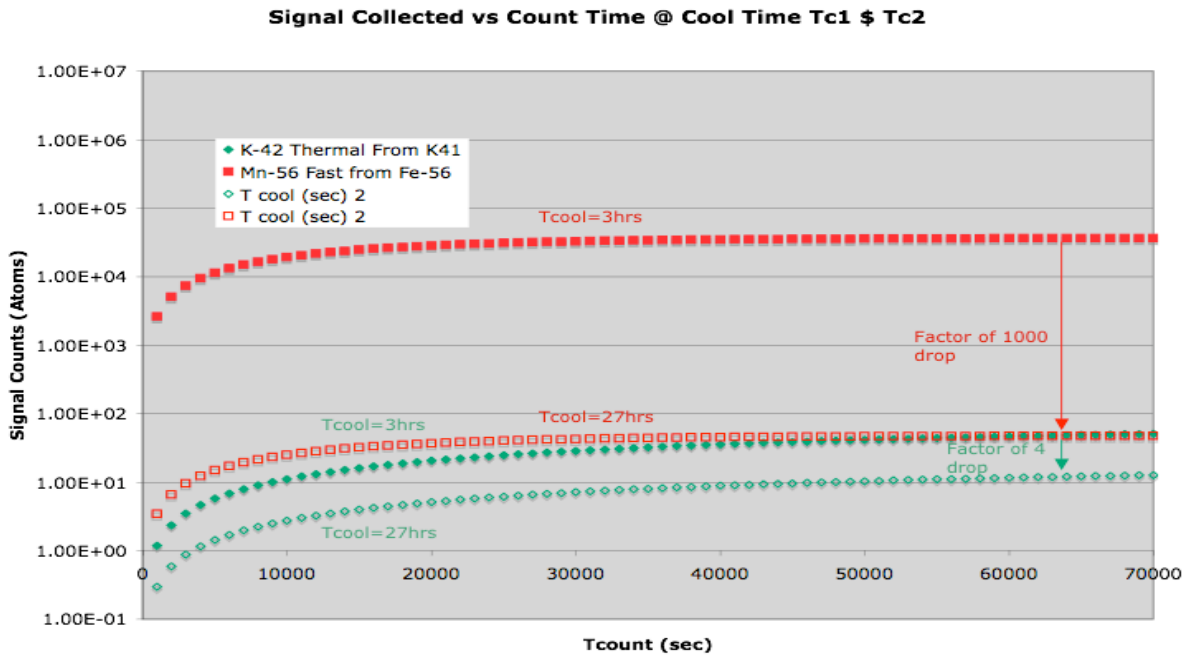
Table V depicts K ppm measured by our reference in Berkeley and that is compared to the upper limit ppm of K we estimated from no signal. The percent error represents the deviation from the .24ppm of K.

Our estimated upper limit on the amount of K in the Ti sample is .0180ppm. This is about a factor of 10 off. Either the direct measurement provided by Berkeley was contaminated or there is an innate flaw in the NAA method, such as the measurement of the thermal flux.

It is important to point out that in our K measurements before, we were able to clearly see peaks that originated from about

.3 to .1ppm of K which is in the same region as the direct measurement given by our reference in Berkeley. Whereas in our case, no matter if the cool time is 3hrs or 27hrs (when the Mn-56 continuum is mostly gone) the K-42 peak is nowhere to be seen. Assuming our upper limit is correct graph VII shows why we couldn't be able to see the peak.

Here with .0180ppm of K and 231ppm of Mn (Exposure=1hr) 15g sample



Graph VII: K-42 (.0180ppm) and Mn-56 (231ppm) Signal Intensities

Here we can see that the intensity of K-42 is always lower than that of Mn-56 and is never seen due to the Mn-56 continuum raising the background above the K-42 peak.

Conclusions/Future Work:

The next step for verification of the NAA method is to build a Ti cylinder with a screw top to hold K contaminants and ensure none fall off. Additionally make sure that the KOH is weighed in a very dry environment to ensure proper measurements of KOH mass and in turn mass of K. This will ensure proper measurement of K that is added to the Ti vial.

Additionally we need to expose a properly seal vial full of only air to confirm the error in the measurement of Argon in the air.

Finally we wish to acquire new flux markers to measure the thermal and fast fluxes of the reactor to ensure those are correct.

These additions should either verify or disprove the NAA methods accuracy.

The current evaluation of the NAA method is that it is a promising method. The Fe ppm was measure fairly accurately (within 9%) and the 2.43 ppm K contaminant measurements were fairly accurate as well (within 7%); however, the .319ppm K measurement and the 6740ppm

Ar measurement were both off by about a factor of 3 (60% and 60.9% respectively). Due to the proper measurements of the 2.43 K contaminant and the 300ppm Fe, it is presumed that some of both the air and .319ppm K were lost between weight measurements and decay signal measurements.

Additionally we have conflicting measurements between two different methods (direct low background counting and the NAA method) where the first method predicts .24ppm K naturally within the Ti samples and our method predicts and upper limit of .0180ppm. Further exposures will be needed to crosscheck these results.

There is still no sign of the Uranium, Neptunium or Thorium decay lines. This is because they are hidden by the Scandium background continuums. The solution to this is to activate less Scandium. This can be done by lowering Fast Neutron Flux by building a heavy water container to block more Fast Neutrons and raise the thermal to fast ratio. This will hopefully allow us to see these hidden lined of interest.

VII. References

References:

^{2,3,5,6,7,10}Krane, Kenneth, David Halliday. *Introductory Nuclear Physics*. 2nd ed. Academic Internet Pub Inc, 2009. 272-373,444-465,788-791. Print.

^{1,9}Wollenberg, Harold , and Alan Smith. "A Concrete Low-Background Counting Enclosure." *Health Physics*. 12.1 Vol. (1966): 53-60. Print.

Firestone, Richard, and Virginia Shirley. *Table of isotopes*. 2 Vols. Wiley-Interscience, 1996. Print.

^{1,9}Alan Smith, Private Communication, 2010

^{2,6}William DeGraffinreid, Private Communication, 2010

^{4,8}Robert Eisberg and Robert Resnick in Quantum Physics of Atoms, Molecules, Solids, Nuclei, and Particles 2nd ed. (John Wiley & Sons, New Dehli, 1985) p. 417-431

Appendix:**A: Flux Calculations****1.5 MW for 3 hours on 06/14**

Use East-1 Silicon-NTD location

Record end of irradiation time

Rabbit A at 0 cm height (reference to bottom of Al connecting tube attached to a wet can)

Sample 1 (bottom)	Ti-1	712.1 mg
Sample 4 (top)	Na ₂ CO ₃ .H ₂ O	21.07 mg (thermal flux)
	Ni	206.5 mg (fast flux)

Rabbit B at 15 cm height

Sample 2 (bottom)	Ti-2	716.7 mg
Sample 5 (top)	Na ₂ CO ₃ .H ₂ O	101.8 mg
	Ni	618.7 mg

Rabbit C at 30 cm height

Sample 3 (bottom)	Ti-1	715.7 mg
Sample 6 (top)	Na ₂ CO ₃ .H ₂ O	506.7 mg
	Ni	1736 mg

- Background count on 50% Ge detector.
- Wait one hour after the end of irradiation before counting samples 1, 2, and 3.
- Count samples 4, 5, and 6 two days after the end of irradiation till ^{58m}Co isomeric transition completes

June 17, 2010

Dave keeps all decay-corrected raw data.

	Na-24	Co-58
0 cm height	30.0 uCi	0.0377 uCi
15 cm height	8.30 uCi	0.0172 uCi
30 cm height	4.64 uCi	0.00974 uCi

Na-23 is about 37% in Na₂CO₃.H₂O; considering all activation is due to thermal neutrons with a cross section of 0.53 b.

Ni-58 is about 68% of natural Ni; using constant 113 mb for (n, p) Co-58.

Therefore, **at 0 cm height**

$$\Phi_{\text{thermal}} * (0.02107 * 37\% / 23) * 0.6e24 * 0.53e-24 * (1 - \exp(-0.693 * 3 \text{ hrs} / 14.96)) / 3.7e4 = 30.0 \text{ uCi}$$

$$\Phi_{\text{thermal}} = 7.9e10 \text{ at 1.5 MW operating power}$$

$$\Phi_{\text{fast}} * (0.2065 * 68\% / 58) * 0.6e24 * 0.113e-24 * (1 - \exp(-0.693 * 3 \text{ hrs} / (70.88 * 24 \text{ hrs}))) / 3.7e4 = 0.0377 \text{ uCi}$$

$$\Phi_{\text{fast}} = 6.9e9 \text{ at } 1.5 \text{ MW operating power}$$

Continue for evaluations at other 2 heights, the following table completes the flux data.

	Φ_{thermal}	Φ_{fast}	$\Phi_{\text{thermal}} / \Phi_{\text{fast}}$
0 cm height	7.9e10	6.9e9	11.4
15 cm height	4.5e9	1.0e9	4.50
30 cm height	5.1e8	2.1e8	2.43

1.5 MW for 1 hour on 06/18

Use East-1 Silicon-NTD location

Record end of irradiation time

Rabbit A at 0 cm height (reference to bottom of Al connecting tube attached to a wet can)

Sample 1 (bottom)	Ti-1	---
Sample 3 (top)	Na ₂ CO ₃ .H ₂ O	62.12 mg (thermal flux)
	Ni	748.9 mg (fast flux)

Rabbit B at 0 cm height (reference to bottom of Al connecting tube attached to a wet can)

Sample 2 (bottom)	Ti-2	---
Sample 4 (top)	Air sample	

June 22, 2010

	Na-24	Co-58
0 cm height	24.4 uCi	0.0393 uCi

 Φ thermal = 6.3e10 at 1.5 MW operating power Φ fast = 6.0e9 at 1.5 MW operating power Φ thermal / Φ fast = 10.5**Observations:****6/14:**

1. Relative Co-58 activities at different heights from Ni-58 (n, p) reactions are similar to Sc-** activities and these data confirm the fast neutron fluxes at different heights.
2. Φ thermal / Φ fast ratios at different heights deteriorate dramatically and this is due to very significant thermal neutron removal by hydrogen in light water. At 0 cm height, the beam line (from core center to samples) passes through the upper portion of the graphite reflector before reaching Rabbit A where the thermal neutron flux remains relatively high.

6/18

3. Flux monitors place on 6/18 are positioned 1" higher than those of the previous run on 06/14 due to a larger Ti sample